Received: 12 May 2023 | Accepted: 29 May 2023

DOI: 10.1002/lio2.1090

ORIGINAL RESEARCH

Laryngoscope Investigative Otolaryngology

Three-dimensionally visualized ossification and mineralization process of the otic capsule in a postnatal developmental mouse

Jing Bai MD | Taku Ito MD | Taro Fujikawa MD | Keiji Honda MD | Yoshiyuki Kawashima MD | Hiroki Watanabe MD | Natsuko Kurata MD | Takeshi Tsutsumi MD

Department of Otolaryngology, Tokyo Medical and Dental University, Tokyo, Japan

Correspondence
Taku Ito, Department of Otorhinolaryngology, Tokyo Medical and Dental University, 1-5-45 Yushima, Bunkyou-ku Tokyo, 113-8519 Japan.
Email: taku.oto@tmd.ac.jp

Funding information
Grant-in-Aid for Scientific Research from Ministry of Health, Labour and Welfare, Grant/Award Numbers: 19K18798, 20K09728, 20K18305, 20K09727, 20K096

Abstract

Objective: We aimed to elucidate the ossification process of the otic capsule in postnatal C57BL/6 mice and depict the three-dimensional (3D) process of otoconial mineralization in vivo.

Methods: The otic capsules of C57BL/6 mice were stained with alizarin red and imaged/compared using micro-computed tomography on postnatal day (P) between P0 and P8, P10, P15, and P30 and 3–4 months old (P3–4Mo). We reconstructed 3D images of the otic capsule and otoconia and measured the bone mineral density using x-ray absorptiometry on each age.

Results: The 3D reconstructed otic capsule images revealed two ossification centers of the otic capsule at P0. One was observed around the ampulla of the superior semicircular canal and utricle, and the other was observed around the ampulla of the posterior semicircular canal. The cross-sectional views demonstrated that modiolar ossification developed from the base to the apex from P4 to P8. The inter-scalar septum ossified bidirectionally from the modiolus and bony otic capsule from P8 to P15. The mineralized otoconia were first detected in the utricle at P3 and saccular otoconia at P6. The density of the utricle and saccular otoconia showed different growth trends.

Conclusion: To the best of our knowledge, this is the first study to demonstrate the 3D appearance of the otic capsule and otoconia in different developmental stages of mice. We also revealed that modiolar and inter-scalar septal calcification is the final event in the cochlea and that it can be susceptible to pathological conditions (cochlear congenital malformations and hereditary vestibular diseases). The unique features of the ossification process and duration may explain these pathological conditions observed in humans.

Level of Evidence: 3

KEYWORDS

3D reconstruction, mineralization, ossification, otic capsule, otoconia

1 | INTRODUCTION

Incomplete partition anomalies represent a group of cochlear malformations in which there is a clear differentiation between the cochlea and vestibule with normal external dimensions but with various internal architectural defects within the cochlea.[1–3] Incomplete partitions are classified into three types according to defects in the modiolus and inter-scalar septa. Incomplete partition type I (IP-I) lacks the entire modiolus and inter-scalar septa. In IP-II, the apical part of the modiolus and the corresponding inter-scalar septa are defective, giving the apex of the cochlea a cystic appearance owing to the confluence of the middle and apical turns. In IP-III, the cochlea has inter-scalar septa; however, the modiolus is completely absent. These cochlear malformations are based on the morphology of the bony labyrinth and generally result from arrest during various stages of embryogenesis. The developmental process of the membranous labyrinth has been extensively studied in mice so far[4]; however, the calcification process of the bony labyrinth (otic capsule) has not been investigated in detail.

The otoconia are bio-crystals composed of $CaCO_3$ and proteins, covering the saccular and utricular maculae. The shape, size, and organization of the $CaCO_3$ crystallites in the otoconia are strictly controlled by an organic matrix composed of proteins and proteoglycans and vary greatly in different regions of the otoconial complex.[5] The development of the majority of the otoconia in the utricular macula occurs on the 15th and 16th gestational days in mice.[6] The gross morphology of the otoconia revealed by scanning electron microscopy is almost complete at birth; however, calcium deposition still continues until postnatal day (P)14.6 It has been shown in various animal models that changes in otolith morphology and reductions in the otolith volume result in vestibular dysfunctions. However, none have reported the nondestructive three-dimensional (3D) developments or quantitative changes in calcium deposition in the otoliths in detail. Thus, this study aimed to elucidate the postnatal ossification process of the mouse otic capsule, modiolus, inter-scalar septa, and otoconia using micro-computed tomography (micro-CT).

2 | MATERIALS AND METHODS

We purchased C57BL/6J mice from Japan SLC (Shizuoka, Japan) and housed them in plastic-bottomed cages with ad libitum access to food and water. This study was approved by the Institutional Animal Care and Use Committee of Tokyo Medical and Dental University (No. A2019-280A). The number of samples used in this study is shown in Table 1.

2.1 | Alcian blue and alizarin red staining

We prepared an Alcian blue solution to stain the cartilaginous tissue using mixtures of Alcian blue 8GX, pH 2.5 (FUJIFILM Wako Pure Chemical Co., 75881231 by CAS), 10 g, and 3% acetic anhydride 1000 mL. Alizarin red S solution (Abcam, ab146374) was prepared for staining the osseous tissue with mixtures of 100 mL sterile water in 1.0-g KOH and 0.5-g alizarin red S solution.[7,8] Mice were euthanized on P0–P8, P10, P15, and P30 and at 3–4 months old (P3–4Mo). We carefully dissected the otic capsules in 0.1-M phosphate-buffered saline (PBS) and fixed them in 4% paraformaldehyde in PBS. Each otic capsule was then stained with Alcian blue solution for 1 day, washed in 95% EtOH for 1–2 h, and soaked in 0.5% KOH (WAKO, 165-21825) overnight, followed by clearing in 1% KOH for 1 day. Subsequently, we stained them with alizarin red S solution diluted in water (1:50) for 2 h or overnight, cleared them in 1% KOH for 1 day, and in 20%, 40%, 60%, 80%, and 100% glycerin, each for 20 min. Finally, we captured images using a stereomicroscope (Olympus SZX 12; Japan).

2.2 | X-ray micro-CT

All samples were imaged using a cone-beam micro-CT (InspeXio SMX-100CT; Shimadzu, Japan).[9,10] The x-ray tube voltage was 75 kV, the tube current was 30 A, the voxel size was 0.01 mm, the total rotation was 360°, and the integration time was 240 s for each stage. The averaging or median filter, ring artifact, or beam hardening correction was not applied during the acquisition (Figure S1). The images were imported into the software InspeXio64 (version 3.0; Shimadzu, Japan) and loaded into the 3D BON software (TRI/3D-BON-FCS; Ratoc System Engineering Co., Ltd.) to measure the bone density of the otic capsule. We processed the images using a free image-processing software program, Image J (v1.53a; National Institutes of Health, USA), and then to a nearly raw raster data (NRRD) file for further 3D reconstruction processing.

2.3 | Otic capsule, bony labyrinth, and otoconium segmentation

We reconstructed the 3D surface images of the otic capsule and otoconium using a 3D slicer (www.3dslicer.com).[11] Yen's method (which was integrated into the software) was used to determine the threshold range.[12,13] Minimal manual adjustments were made when dealing

TABLE 1 Number of samples analyzed.

	Surface Staining (Figure 1)	Micro-CT (Figure 1–3, 5)	BMD measurement (Figures 4 and 6)
P0	7	5	3
P1	6	4	4
P2	6	5	6
P3	2	1	/
P4	6	6	4
P5	1	1	1
P6	4	4	2
P8	5	4	4
P10	/	1	1
P15	/	7	4
P30	/	4	4
P3–4Mo	/	5	5

with the images of the early postnatal mouse specimens. Each surface image of the otic capsule was superimposed on the internal surface of the mature bony labyrinth. The internal surface of the mature bony labyrinth was created using a semiautomatic segmentation algorithm, "Grow from seeds," to extract the models of the intra-otic capsule structures using a 3-month-old mouse.[14] The detailed procedure was described as previously.[10] No user input by code was required to compute the segmentation.

2.4 | Bone mineral density

We also performed 3D reconstruction imaging of the bone system (TRI/3D-BON, RATOC System Engineering Co., Ltd.) to compare and quantify the bone mineral density (BMD) of the otic capsules, semicircular canal, and otoconia. The phantoms that consisted of aluminum and seven types of hydroxyapatite (content, 200, 300, 400, 500, 600, 700, 800, and 1550 mg/cm^3) were scanned under the same conditions as the

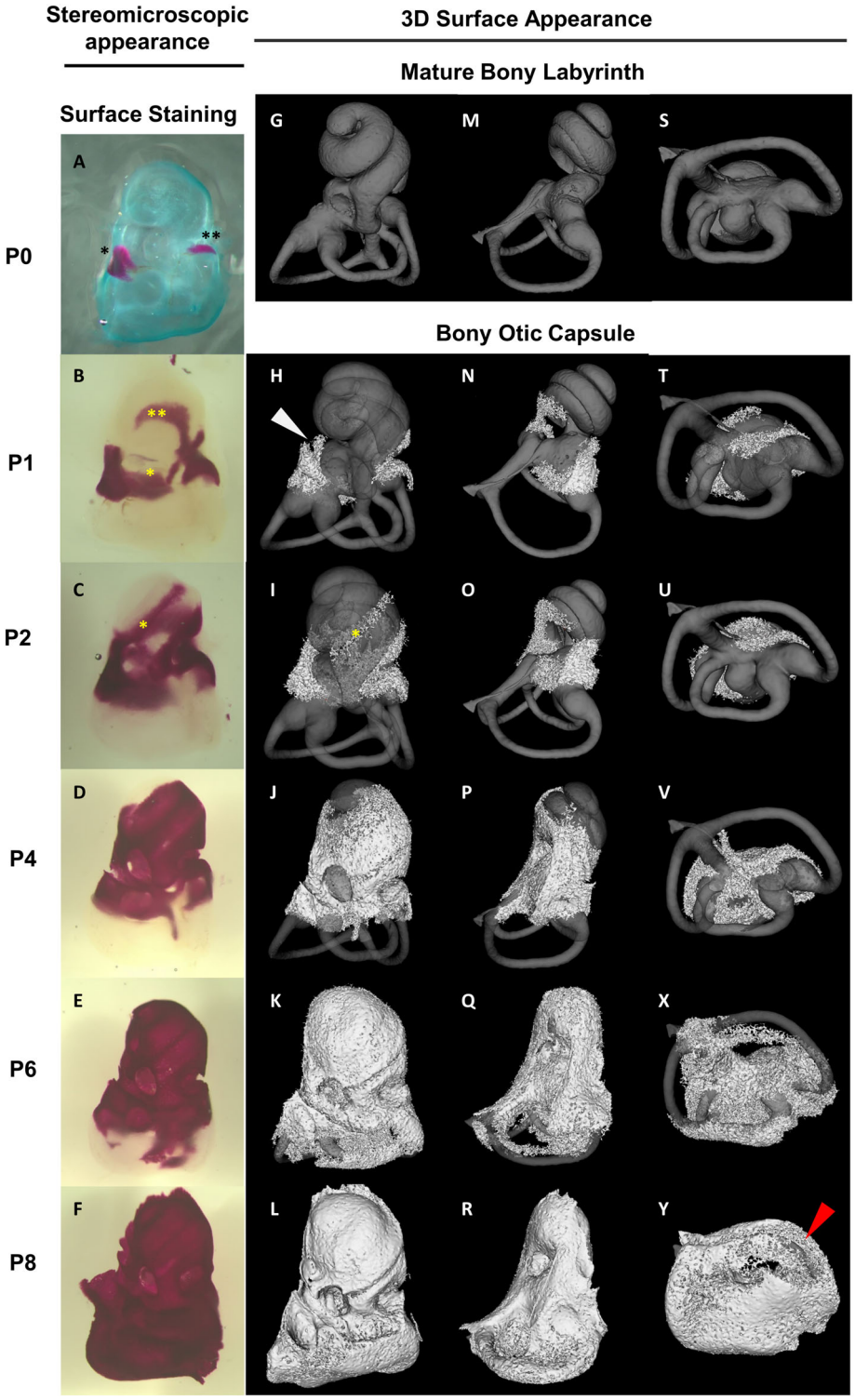

FIGURE 1 Stereomicroscopic and reconstructed computed tomography appearances of otic capsule ossification. Panel a shows that at P0, the otic capsule ossification starts from two distinct locations. One ossification center is observed around the ampulla of the anterior semicircular canal and utricle (asterisk in panels A and B). It then grows toward the saccule (asterisk in panel B) and cochlear middle turn (asterisk in panels C and I). The facial nerve notch is observed (arrowhead in panel H). The other center is identified around the ampulla of the PSCC (double asterisk in panels A and B) and then grows to the cochlear basal turn (double asterisk in panel B). Panels C, I, and O show two integrated ossification centers. The osseous oval window's morphology starts to form. Panels D, J, and P show that at P4, most of the cochlea and the three ampulla were ossified, and panel V shows that the semicircular canal ossification starts from the ampulla. Panels E, K, and S show that at P6, the semicircular canals and round window niche are gradually covered by osseous. Panels F, L, R, and Y show that at P8, the ossification of the semicircular canals is almost completed, except for that of the superior semicircular canal (arrow in y). Panels G, M, and S show a bony labyrinth constructed by the mature otic capsule without ossification at the age of 3–4 months for the superimposed display. Panels M–R show the lateral views of the semicircular canal ossification. Panels S–V show the bottom views of the semicircular canal ossification.

samples (tube voltage, current, and magnification power). A calibration curve of the mean CT intensity and BMD was generated by TRI/3D-BON software (Figure S2a, b). TRI/3D-BON software created the BMD color-mapped images from the micro-CT image of each sample according to the calibration curve and calculated the BMD values of the whole otic capsules (Figure S2c, d). A phantom image of known density was used to calibrate the linear regression slope (Figure S2a, b). In addition, the BMD of the otoconia and ampulla of the posterior semicircular canal (PSCC), which is one of the primary ossification centers, was quantified using ImageJ. We took 6–12 points randomly around the site of the ampulla of the PSCC and otoconium at each age and calculated the mean pixel value. To calculate the BMD value, we used the calibration linear regression equation mentioned earlier.

3 | RESULTS

3.1 | Surface ossification process of the otic capsule

Alizarin red staining (Figure 1A–F) revealed that otic capsule ossification started from two distinct locations at birth (Figure 1A). At P1, they multi-directionally developed into both the vestibular and cochlear parts (Figure 1B). From P2 to P4, the alizarin red-stained area of the cochlear part gradually progressed from the basal to middle turns but not to the apical turns. The stained area of the vestibular part developed around the overall otolith organs but not around the semicircular canals or vestibular aqueduct at P4. The stained area of the otic capsule reached the top of the cochlear turn at P6 and spread throughout P8, including all semicircular canals and vestibular aqueducts.

The 3D reconstructed surface images (Figure 1G–Y) combined with the superimposed internal surface of the mature labyrinth display revealed that the ossification center observed at P0, marked by an asterisk in Figure 1A, was around the ampulla of the superior semicircular canal (SSCC) and utricle (Figure 1A, H). It appeared to spread to most portions of the vestibule from P0 to P2 (Figure 1A–c and 1H,I and Figure S3). Another center labeled with a double asterisk in Figure 1A was detected around the ampulla of the PSCC (Figure 1A, H) and appeared to develop on the outer appearance of the cochlea and inter-scalar septum of the basal turn (Figure 1A–C and 1H,I and Figure S3) at P2. The ossification process of the cochlea progressed from the basal to apical turns (Figure 1H,I) alongside each inter-scalar septum at P2, and two ossification centers joined to each other. The bony outer appearance of the cochlea was observed to be complete at P6 (Figure 1K). The ossification around the otolith organs occurred around P4 and was restricted around three ampulla (Figure 1J, P, V). At P6, the ampulla in the semicircular canals ossified, followed by the common crus and canals (Figure 1K, Q, X). The ossification of the semicircular canals was nearly developed, except for the SSCC at P8 (Figure 1L, R, Y). We used more than three mice at P0, P1, P2, P4, P6, and P8 to see the stained area and mode of Alcian blue and alizarin

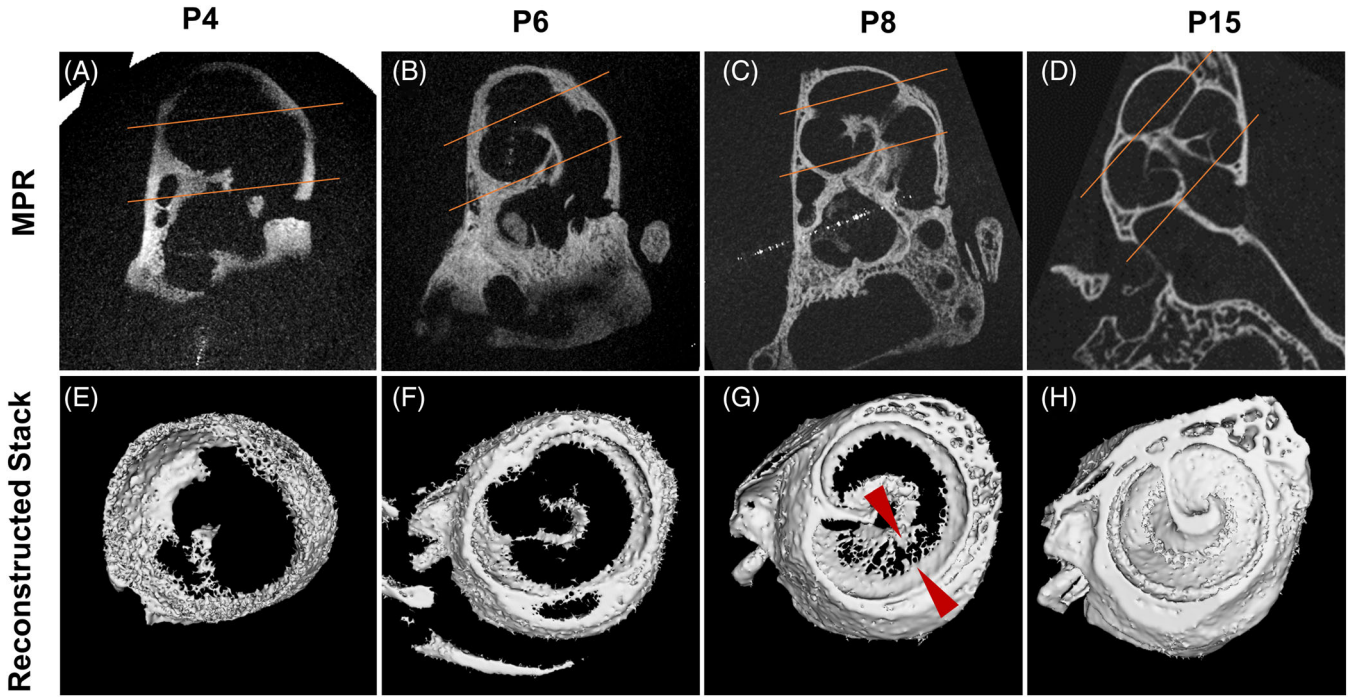

FIGURE 2 Cross-sectional views of the osseous cochlea. Panels A–D show the multiple-planner reconstructed images of the cochlear mid-modiolar sections. Panels E–H show the three-dimensional views from the topside when cropping the reconstructed images of Figure 1L–N, and one at P15 along the red line. At postnatal day (P)4, the ossification of the modiolus starts around the bottom of the cochlea (A, E). At P6, it superiorly grows to the apex (B, F). At P8, the ossification of the modiolus is almost completed; however, the inter-scalar bony septa do not sufficiently ossify. Inter-scalar septa ossification progresses laterally from the modiolus and medially from the bony outer otic capsule (arrows in g). At P15, the ossification of the modiolus and inter-scalar septa is completed (D, H).

red and to create the 3D surface images by micro-CT and verified their reproducibility. The mode of calcification development was similar among individual samples, and the calcification degree of the otic capsule at each age was within a difference of 1–2 days.

3.2 | Modiolus and cochlear partition ossification

The cross-sectional views on micro-CT demonstrated that modiolar ossification began around the bottom of the cochlea at P4 (Figure 2A). It developed from the base to the apex at P8 (Figure 2B,C). In contrast, the inter-scalar bony septa did not appear to grow at P6 (Figure 2F). The inter-scalar septa ossified laterally from the modiolus and medially from the bony otic capsule at P8–P15 (Figure 2C,D,G,H). At P15, the inter-scalar bony septa connected and almost completed (Figure 2D, H). The 3D reconstruction views demonstrated that the modiolus originated from the ossification center (labeled with a double asterisk in Figure 3A) corresponding to a double asterisk in Figure 1A, B. At P4, the ossification of the modiolus was limited to the basal end of the cochlea (Figure 3B) and considerably ossified at P5 (Figure 3C). The BMD images

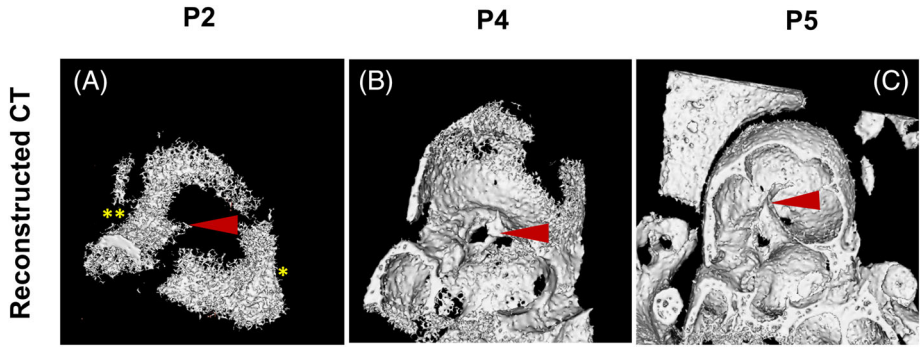

FIGURE 3 Cross-sectional views of the osseous cochlea in a vertical view. The cross-sectional views demonstrate that the modiolus is limited at postnatal day (P)4 (b). Panel C shows that the modiolus is considerably ossified at P5, and the bony outer appearance of the cochlea is fully covered. The asterisk indicates the primary ossification center around the ampulla of the anterior semicircular canal and utricle. The double asterisk indicates the primary ossification center around the ampulla of the posterior semicircular canal. The arrows show the modiolus.

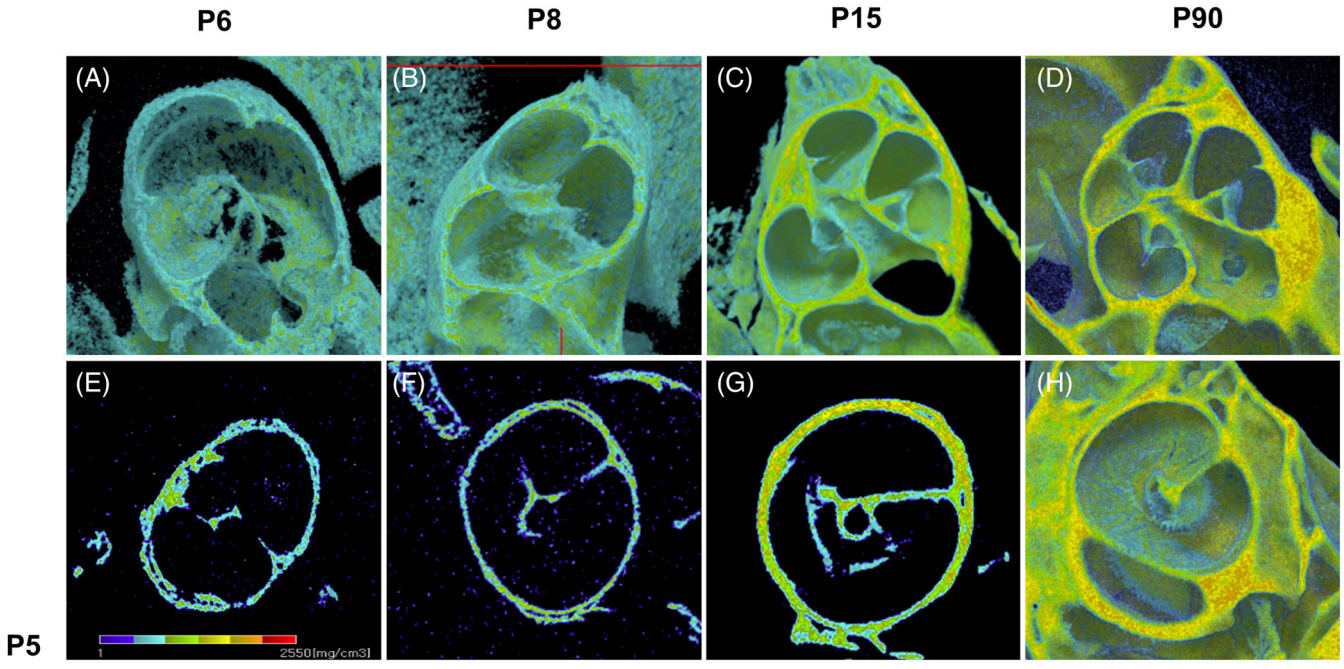

FIGURE 4 Bone mineral density (BMD) image views of the osseous cochlea. The true value of the BMD is visualized according to the calibration curve of a phantom. The colors purple, sky blue, green, yellow, orange, and red correspond to the BMD value from 1 to 2550 mg/cm^3 in order. Panels A–D show the three-dimensional reconstructed images of the cochlear mid-modiolar sections. Panels E–H show the views of two-dimensional cross-section from the topside. At postnatal day (P)5 and P6, both the outer side of the otic capsule and modiolus are sky blue. At P8, green is increased (B, F). At P15, the ossification of the modiolus and inter-scalar septa is completed, and both yellow and green are filled in both spaces of the outer otic capsule and modiolus. At 3–4 months old, orange is filled in the bony structure, and there is little blue in the inter-scalar septa (D, H).

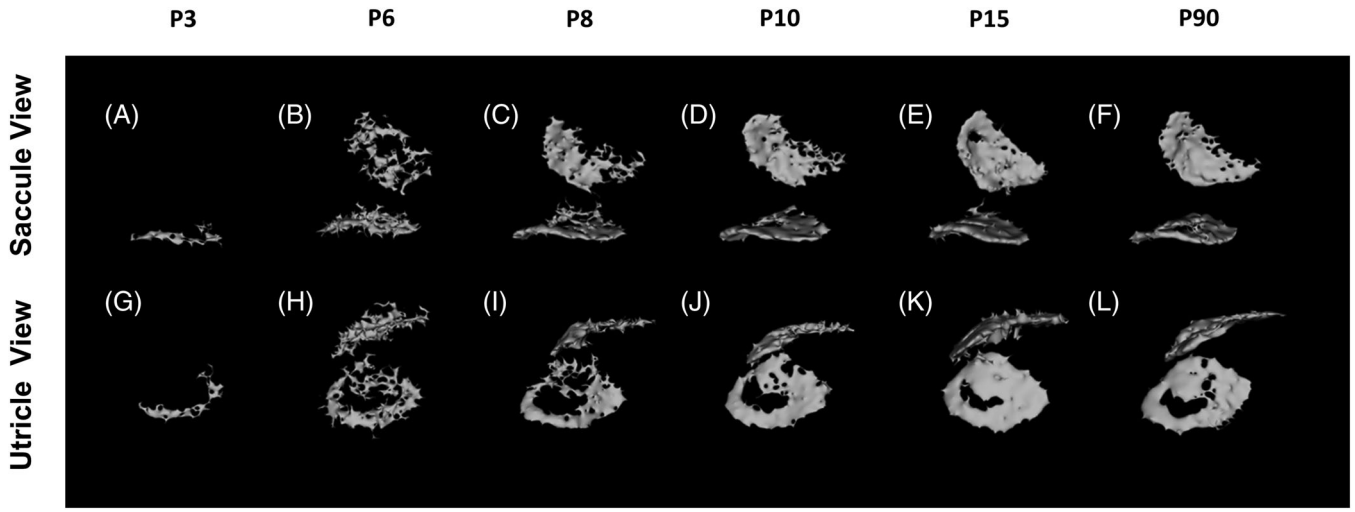

FIGURE 5 Otoconium calcification. The utricular otoconia are first detected at P3 by reconstructed micro-computed tomography (A, G), whereas the saccular otoconia are identified at P6 (B, H). The otoconium calcification gradually develops between P6 and P10, and the calcium depositions on the otoconia on the utricle and saccule are almost completed at P15 (E, K), the computed tomography images of which are almost identical to those at P3–4Mo (F, L).

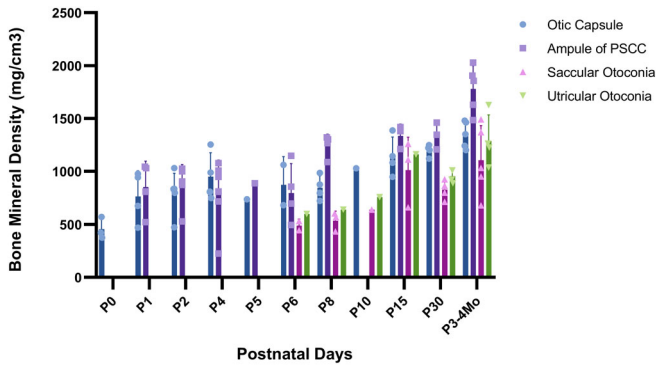

FIGURE 6 The bone mineral density (BMD) of the otic capsule and density of the otoconial layers. The BMD of the otic capsule increases continually from postnatal day (P)0. From P0 to P2, the BMDs of the otic capsule and ampulla of the PSCC remain similar. The otic capsule only ossifies the original parts. After P8, the BMD of the ampulla of the PSCC surpasses the BMD of the otic capsule. The otic capsule is almost completed at P8. The densities of both the utricular and saccular otoconia gradually increase, whereas they are all less than that of the otic capsule. The error bar represents the standard deviation.

of the osseous cochlea showed the mineralization process of the modiolus and inter-scalar septa (Figure 4). The modiolus was green (approximately 800 mg/cm^3) at P8 (Figure 4B, F), and the inter-scalar septa were green at P15 (Figure 4C, G).

3.3 | Otoconial mineralization

The otoconium was first detected in the utricle at P3 by reconstructed micro-CT (Figure 5A,G), whereas the saccular otoconium was identified at P6 (Figure 5B, H). The calcium of the otoconia was almost deposited on the utricle and saccule at P15, and the CT images of the otoconia at P15 were almost identical to those at P3–4Mo (Figure 5F,L).

3.4 | BMD increment of the otic capsule and otoconia

The BMD of the otic capsule increased continually from P0, at around 500 mg/cm^3, until P3–4Mo, when this value increased to above 1000 mg/cm^3 (Figure 6). From P0 to P2, the BMDs of the otic capsule and ampulla of the PSCC were similar. The otic capsule only ossified the original parts. After P8, the BMD of the ampulla of the PSCC surpassed that of the otic capsule. The otic capsule was almost completed at P8. The densities of both utricular and saccular otoconia continued to increase until P3–4Mo, at around 1000 mg/cm^3(Figure 6).

4 | DISCUSSION

To the best of our knowledge, this is the first study to demonstrate the 3D ossification process of the otic capsule in developing mice using micro-CT. The 3D reconstruction affords spatial construction information, which is difficult to recognize on the two-dimensional sectional views. We revealed the primary ossification areas of the otic capsule and spatial mineralization trends of the modiolus and scalar septum. In addition, we quantified the rate of calcium deposits and illuminated the developmental patterns of the otoconia. We found that alizarin red staining and micro-CT showed similar results in identifying the ossification process. Micro-CT evaluates calcium deposition based on x-ray permeability, whereas alizarin red directly detects calcium deposition. Alizarin red staining combined with alcian blue

staining facilitated the spatial orientation of the calcification sites, which was superior to micro-CT, especially for early postnatal otic capsules. In contrast, the nondestructive 3D evaluation and assessment of the degree of calcification were solely possible using micro-CT. It was effective to evaluate both methods in the current study. Micro-CT images did not completely match the alizarin red-stained area. Our threshold segmentation method delineated slightly different boundaries compared with those detected by alizarin red staining.

During the fourth to fifth fetal months in humans, ossification of the otic capsule commences after the surrounding cartilage has attained its final shape and size, which corresponds to the developed membranous labyrinth. Calcium deposition starts from the center of ossification at the 16th to 21st weeks of fetal life. Bast et al. identified 14 primary ossification centers and numbered them using histological sections. Four centers initially appeared in the cochlea and ampulla of the SSCC at the 16th week. The next nine centers were present around the internal acoustic meatus and between the vestibule and cochlea at the 18th week. The last appeared over the crus of the posterior canal at the 21st week.[15] In our study, we identified two distinct earliest ossification centers in the otic capsule of mice. They are likely corresponding to ossification centers 3 and 1 or 2 (Figure S4). The 3D reconstruction of micro-CT revealed that the mouse otic capsule ossified from two centers located primarily on the ampulla of the semicircular canals followed by the vestibule and cochlea. This trend of calcium deposition was consistent with that in the human temporal bone by decalcified sections[15]; however, the other remaining centers could not be identified in mice. Further studies are needed to determine the number of central points in the human otic capsule where calcium deposition begins.

The progression of mineralization in the modiolus of humans was previously reported to begin at 20 weeks' gestation. However, the detailed 3D ossification process of the modiolus has not been described. The current study revealed that ossification of the mouse modiolus started around the basal turn at P4 (Figure 2A). From P5 to P6, it rapidly elongated in the apical direction in a spiral manner but did not reach the apical end at the time when the bony appearance of the otic capsule had already been fully covered. Modiolar ossification spread to the end of the apical turn at P8 (Figure S5). In contrast, the BMD rapidly increased from P6 to P8, similar to areas in the otic capsule. These results imply that calcium deposition in the modiolus occurs simultaneously with elongation, whereas calcium deposition on the other site of the otic capsule spreads slowly throughout the early stage and then rapidly increases in the late stage. This difference may be because the morphogenesis of the modiolus differs from that of other parts of the otic capsule. In humans, no cartilage is observed in the modiolus at any of the fetal stages.[15] The modiolus is formed from a type of membranous bone with spicules of bone formation and not from the endochondral bone.[1,15] Similarly, most of the inter-scalar septum is formed by intramembranous bone formation from the modiolus. The inter-scalar septum separates each turn of the cochlea from the contiguous turn. Thus, the scala vestibule of the first cochlear turn is separated from the scala tympani of the second turn by the inter-scalar septum. Therefore, separation of the cochlear duct at the apical turn occurs during the delayed period, which is consistent with our findings in mice (Figure 2). We hypothesized that the difference in ossification speed may be due to the difference between the intramembranous and intra-cartilaginous processes, and the apical inter-scalar septum could be more susceptible to pathological conditions.

Micro-CT can obtain precise information with minimal artifacts; however, it is difficult to quantitatively analyze the density of the otoconia because of its low radiodensity, which makes it technically challenging to determine the boundary to separate the otoconia from the background.[16] We partially resolved this problem using the automatic artificial intelligence algorithm, "keep selected island" in the 3D slicer, by which the otoconia would be separated from the background without manual work (Figure 5). In addition, we performed a quantitative analysis of the otoconial layer to understand saccular and utricular calcium deposition development under identical photo and processing conditions. The normal formation of the otoconia requires the correct homeostasis of the saccular and utricular endolymph and increasing calcium and bicarbonate concentrations locally in a specific order and time. If not, the otoconia result in irregularly shaped inorganic crystals, leading to severely impaired balance function.[5] The lack of formation of giant otoconia in saccular otoconia has been reported in *Slc26a4*-null mice,[12,17] in which endolymphatic homeostasis has been broken.[18] An important role of hair cells has also been suggested in the maintenance of the otoconia.[19,20] Plasma membrane calcium ATPase 2 (PMCA2) is expressed in the outer hair cells and has been implicated in the maintenance of the endolymph calcium concentration.[21] The saccular otoconia have disappeared at the age of 1 month in *PMCA2 type 2* gene-null mice.[16]

The reconstructed CT demonstrated that the otoconia in the lateral region of the utricular otoconial layer were first detected and the center of the otoconial layer was not detected. This trend was still present in the mature inner ears, probably due to the limited resolution and signal-to-noise ratio. The mean size of the otoconia is approximately 10 μm,[22] whereas the minimum voxel size of the reconstructed CT dataset was 5 μm in our study. However, it was impossible to completely differentiate the signal from the background noise using any option of the 3D slicer algorithm. More detailed observations of the otolith developmental patterns and ectopic otoconia are required in the advent of more sophisticated instruments.

This study has some limitations. First, micro-CT took clear images of the otoconium on postnatal days. However, the otoconium images were obscure and unmeasurable in adult mice. Our technical method could not provide sufficient contrast through a thick otic capsule. Second, we performed the morphological analysis of the ossification and mineralization processes; therefore, we could not determine the relationship with various signaling molecules, including TGF, BMP, and FGF. Furthermore, in the future, we would aim to conduct molecular embryogenesis research to reveal how it leads to the normal shape formation of the otoconia and otic capsule.

5 | CONCLUSION

In the inner ear, vestibular/semicircular development precedes cochlear organ development; however, the current study revealed calcification of the cochlea prior to the semicircular canals. Our results

clearly revealed the 3D osseous labyrinth ossification and otoconial mineralization process using reconstructed micro-CT. The unique features of the ossification process and duration may explain the pathological conditions of cochlear congenital malformations and hereditary vestibular diseases observed in humans.

ACKNOWLEDGMENTS

We are grateful to Dr. Ayane Makabe, Dr. Ayako Maruyama, Dr. Natsuki Aoki, and Dr. Tomoki Ooka for their helpful discussions.

CONFLICT OF INTEREST STATEMENT

The authors declare no conflict of interest.

DATA AVAILABILITY STATEMENT

The raw data supporting the conclusions of this article will be made available by the authors, without undue reservation.

ORCID

Taku Ito https://orcid.org/0000-0002-8368-9573
Taro Fujikawa https://orcid.org/0000-0002-3251-9080

REFERENCES

1. Sennaroğlu L, Bajin MD. Classification and current management of inner ear malformations. *Balkan Med J*. 2017;34:397-411.
2. Sennaroglu L, Saatci I. A new classification for cochleovestibular malformations. *Laryngoscope*. 2002;112:2230-2241.
3. Jackler RK, Luxfor WM, House WF. Congenital malformations of the inner ear: a classification based on embryogenesis. *The Laryngoscope*. 1987;97:2-14.
4. Morsli H, Choo D, Ryan A, Johnson R, Wu DK. Development of the mouse inner ear and origin of its sensory organs. *J Neuroscience*. 1998;18:3327-3335.
5. Hughes I, Thalmann I, Thalmann R, Ornitz DM. Mixing model systems: using zebrafish and mouse inner ear mutants and other organ systems to unravel the mystery of otoconial development. *Brain Res*. 2006; 1091:58-74.
6. Nakai Y, Chang KC, Morimoto A, Morisaki N. An experimental study of the development and pathogenesis of Otoconia. *Practica Oto-Rhino-Laryngologica*. 1982;75:135-143.
7. Dror AA, Lenz DR, Shivatzki S, Cohen K, Ashur-Fabian O, Avraham KB. Atrophic thyroid follicles and inner ear defects reminiscent of cochlear hypothyroidism in Slc26a4-related deafness. *Mammalian Genome*. 2014;25:304-316.
8. Wangemann P, Kim H-M, Billings S, et al. Developmental delays consistent with cochlear hypothyroidism contribute to failure to develop hearing in mice lacking Slc26a4/pendrin expression. *Am J Physiol-Ren Physiol*. 2009;297:F1435-F1447.
9. Elfarnawany M, Alam SR, Rohani SA, Zhu N, Agrawal SK, Ladak HM. Micro-CT versus synchrotron radiation phase contrast imaging of human cochlea. *J Microsc*. 2017;265:349-357.
10. Ito T, Fujikawa T, Honda K, et al. Cochlear Pathomorphogenesis of incomplete partition type II in Slc26a4-null mice. *J Assoc Res Otolaryngol*. 2021;22:681-691.
11. Velazquez ER, Parmar C, Jermoumi M, et al. Volumetric CT-based segmentation of NSCLC using 3D-slicer. *Scientific Rep*. 2013;3: 3529.
12. Ito T, Honda K, Watanabe H, et al. Morphometric analysis of the otic capsule and otoconia in a mouse model of Pendred syndrome using X-ray computed microtomography. *Equilibrium Res*. 2020;79: 236-243.
13. Yen JC, Chang FJ, Chang S. A new criterion for automatic multilevel thresholding. *IEEE Trans Image Process*. 1995;4:370-378.
14. Vezhnevets V, Konouchine V. GrowCut: Interactive multi-label ND image segmentation by cellular automata *proc. of Graphicon*: Citeseer, 2005:150–156.
15. Anson BJ, Bast TH, Cauldwell EW. LIV the development of the auditory Ossicles, the Otic capsule and the extracapsular tissues. *Ann Oto Rhinol Laryngol*. 1948;57:603-632.
16. Honda K, Noguchi Y, Kawashima Y, Takahashi M, Nishio A, Kitamura K. Ex vivo visualization of the mouse otoconial layer compared with micro-computed tomography. *Otol Neurotol*. 2015;36: 311-317.
17. Everett LA, Belyantseva IA, Noben-Trauth K, et al. Targeted disruption of mouse Pds provides insight about the inner-ear defects encountered in Pendred syndrome. *Hum Mol Genet*. 2001;10: 153-161.
18. Wangemann P, Nakaya K, Wu T, et al. Loss of cochlear HCO3- secretion causes deafness via endolymphatic acidification and inhibition of Ca2+ reabsorption in a Pendred syndrome mouse model. *Am J Physiol Renal Physiol*. 2007;292:F1345-F1353.
19. Minck DR, Erway LC, Vorhees CV. Preliminary findings of a reduction of otoconia in the inner ear of adult rats prenatally exposed to phenytoin. *Neurotoxicol Teratol*. 1989;11:307-311.
20. Takumida M, Zhang DM, Yajin K, Harada Y. Formation and fate of giant otoconia of the Guinea pig following streptomycin intoxication. *Acta Otolaryngol*. 1997;117:538-544.
21. Shull GE, Okunade G, Liu LH, et al. Physiological functions of plasma membrane and intracellular Ca2+ pumps revealed by analysis of null mutants. *Ann N Y Acad Sci*. 2003;986:453-460.
22. Walther LE. Otokonien. *Hno*. 2016;64:767-776.

SUPPORTING INFORMATION

Additional supporting information can be found online in the Supporting Information section at the end of this article.

How to cite this article: Bai J, Ito T, Fujikawa T, et al. Three-dimensionally visualized ossification and mineralization process of the otic capsule in a postnatal developmental mouse. *Laryngoscope Investigative Otolaryngology*. 2023;8(4): 1036-1043. doi:10.1002/lio2.1090